



HAL
open science

The assistance of BAZAR robot promotes improved upper limb motor coordination in workers performing an actual use-case manual material handling

Tiwana Varrecchia, Giorgia Chini, Sonny Tarbouriech, Benjamin Navarro, Andrea Cherubini, Francesco Draicchio, Alberto Ranavolo

► To cite this version:

Tiwana Varrecchia, Giorgia Chini, Sonny Tarbouriech, Benjamin Navarro, Andrea Cherubini, et al. The assistance of BAZAR robot promotes improved upper limb motor coordination in workers performing an actual use-case manual material handling. *Ergonomics*, inPress, 10.1080/00140139.2023.2172213 . hal-04370105

HAL Id: hal-04370105

<https://hal.science/hal-04370105>

Submitted on 3 Jan 2024

HAL is a multi-disciplinary open access archive for the deposit and dissemination of scientific research documents, whether they are published or not. The documents may come from teaching and research institutions in France or abroad, or from public or private research centers.

L'archive ouverte pluridisciplinaire **HAL**, est destinée au dépôt et à la diffusion de documents scientifiques de niveau recherche, publiés ou non, émanant des établissements d'enseignement et de recherche français ou étrangers, des laboratoires publics ou privés.

The assistance of Bazar robot promotes improved upper limb motor coordination in workers performing an actual use-case manual material handling

Tiwana Varrecchia¹, Giorgia Chini^{1,*}, Sonny Tarbouriech², Benjamin Navarro², Andrea Cherubini², Francesco Draicchio¹, Alberto Ranavolo¹

¹ Department of Occupational and Environmental Medicine, Epidemiology and Hygiene, INAIL, 00078 Rome, Italy; t.varrecchia@inail.it (T.V.); g.chini@inail.it (G.C.); f.draicchio@inail.it (F.D.); a.ranavolo@inail.it (A.R.)

² LIRMM, Univ Montpellier, CNRS, Montpellier, France. Emails: sonny.tarbouriech@gmail.com (S.T.); benjamin.navarro@lirmm.fr (B.N.); andrea.cherubini@lirmm.fr (A.C.)

*Corresponding author: g.chini@inail.it

Abstract: This study aims at evaluating upper limb muscle coordination and activation in workers performing an actual use-case manual material handling (MMH). The study relies on the comparison of the workers' muscular activity while they perform the task, with and without the help of a dual-arm cobot (BAZAR). Eleven participants performed the task and the flexors and extensors muscles of the shoulder, elbow, wrist, and trunk joints were recorded using bipolar electromyography. The results showed a reduction in both upper limb and trunk muscle co-activation and activation when the specific MMH was performed with BAZAR. Therefore, Human-robot collaboration technologies, which share the workspace with workers, offload workers from external loads and improve the task execution efficiency and quality. Furthermore, they also allow a better coordination and reduce the worker's physical effort while s/he physically interacts with the robot, and positively affect his/her physiological motor strategy.

Practitioner Summary: Upper limb and trunk muscle co-activation and activation is reduced when a specific manual material handling was performed with a cobot than without it. By improving coordination, reducing physical effort and changing motor strategy, cobots could be proposed as an ergonomic intervention to lower workers' biomechanical risk in industry.

Keywords: Human-robot collaboration, motor coordination, manual material handling, sEMG.

1. Introduction

Some of the fourth industrial revolution (industry 4.0) technologies are creating a new way of working (Lenz et al., 2008), leading towards occupational changes (Baltrusch et al., 2021; Pauliková et al., 2021) and implying a wide-sweeping transformation of the whole productive system (Paolillo et al., 2022). In particular, human labor will be increasingly assisted in a variety of industries and manufacturing (Ito et al., 2022). Such assistance is a viable option for ergonomic interventions for lowering biomechanical risk in manual material handling (MMH) (World Robotics, 2019; Ajoudani et al., 2020). Human-robot collaboration (HRC) technologies, artificial intelligence (Pauliková et al., 2021; Schwab, 2017) and wearable wireless miniaturized sensors (Ranavolo et al., 2018; Alberto et al., 2018) are among the physical and digital systems enabling this transformation. In fact, they allow workers to be physically assisted and monitored, even during demanding occupational tasks. HRC technologies are meant to share the workspace with workers, to continually communicate with them, to manage the human partner's flexibility and ergonomics and to physically interact, in order to jointly work together on a common goal (Behrens et al., 2015). Reconfigurable collaborative robots quickly adapt to the workers' intentions and task variations, while simultaneously offloading them from external loads (task-related payloads) and keeping them in ergonomic working circumstances, to improve efficiency and quality of the task execution (SOPHIA project, <http://www.project-sophia.eu>). Wearable sensors attached to the workers body (e.g., inertial measurement units - IMUs, insoles for measuring reaction forces and bipolar and high-density surface electromyography sensors - sEMG, 3D depth cameras, etc.) measuring his/her motion can greatly improve the accuracy and precision of the biomechanical evaluation, via data-model fusion and machine learning techniques (Varrecchia et al., 2022, 2021, 2020, 2018; Ranavolo et al., 2020a, 2020b, 2018, 2017a, 2017b).

Although there exist many hypotheses and scientific evidence regarding the beneficial effects of HRC, more research into human side effects is required. In this new collaborative scenario, human dexterity and flexibility are paired with the repeatability and precision of a robot, resulting in a reduction in human effort (Ogenyi et al., 2021; Brookham et al., 2016; Salvini et al., 2011) but also in an alteration of human motor strategy. From a broad perspective, although collaborative work (for example, annex A of ISO/DIS 11228-1) is a widespread method for lowering work-related musculoskeletal disorders (WMDs), the scientific literature reveals conflicting findings on its efficacy, due to factors affecting team capacity, autonomy, and coordination (Chini et al., 2022; Anton et al., 2013; van der Molen et al., 2012; Faber et al., 2012; Kim et al., 2012; Barret and Dennis, 2005; Lee, 2004; Dennis and Barret, 2003a, 2003b, 2002; Lee and Lee, 2001). In the latter case, the team must flawlessly coordinate, whereas a single individual can move the load freely and smoothly. To measure motor coordination in body segments and joint stabilization during dynamic tasks, a common approach is muscle co-activation (Chini et al., 2022; Le et al., 2017, Ranavolo et al., 2015; 2018; Granata and Marras, 2000). Compressive and shear forces across the joints increase when significant antagonist activations counteract the agonist actions, producing moments which do not contribute to the required net joint moments (Lewek et al., 2004; Childs et al., 2004; Griffin and Guilak, 2005; Collins et al., 2011). Then, co-activation may become functionally unfavorable (Macaluso et al. 2002; Brookham et al., 2011). For this reason, the use of HRC technologies must be proved primarily during sub-tasks in which the worker physically interacts with the robot, affecting the physiological motor strategy.

Furthermore, no evidence of a motor coordination improvement exists even when the assistance is provided by an advanced collaborative robot (cobot) capable of bimanually handling a heavy object, while simultaneously moving in the workspace. Indeed, even though cobots are a potentially useful tool for enhancing worker ergonomics and are frequently used in assembly-line production environments (Ajoudani et al., 2020; Shi et al., 2012; Papakostasa et al., 2011; Makrini et al., 2018), they tend to focus on lightweight tasks and are rarely in direct physical contact with humans. Indeed, they

only share a workspace with their human partners. In our study, we developed and evaluated a more ambitious scenario in which the cobot works directly in contact with people on a high payload operation. The effectiveness of this collaboration needs to be evaluated not only in the reduction of physical effort, but also in the altered motor strategy adopted by the worker. In fact, the physical interaction could also lead to an ineffective motor strategy which could induce, for instance, upper-arm stiffness. Indeed, collaborative tasks have been shown to introduce critical issues related to autonomy, team skills and coordination between team members (Chini et al., 2022; Anton et al., 2013; van der Molen et al., 2012).

Since, to the best of the authors' knowledge, no research has been done on upper limb co-activation and muscle activation during a hybrid worker-robot MMH, we hypothesize this collaboration may reduce upper limb muscle co-activation and muscular activation. Furthermore, we believe that studying the human-robot interaction throughout the execution of a real-world use case, extrapolated and recreated from an industrial context, will allow us to draw more general conclusions regarding its efficacy.

As a result, the purpose of this research was to evaluate upper limb muscle coordination and activation in workers performing an actual use-case MMH, by comparing a scenario where the workers are helped by a dual-arm cobot with a scenario without the cobot.

In this work, since high payloads (above 15 kg) are incompatible with most current day CoBot arms (Elprama et al., 2017), we relied on the dual-arm mobile cobot BAZAR (Cherubini et al., 2019), which is equipped with two 7-DOF Kuka LWR4 arms attached to a Neobotix MPO-700 omnidirectional mobile base. A Microsoft Kinect camera is mounted on BAZAR's head, and an ATI Mini 45 force/torque sensor is mounted on each of the robot's wrists. Each wrist is also equipped with a 3D printed concave part, designed to fit the shape of the part to manipulate, and denoted 'hand' in the rest of the paper. BAZAR is being assessed as a cobot in the context of "SOPHIA—Socio-Physical Interaction Skills for Cooperative Human–Robot Systems in Agile Production", a project funded by the European Union's Horizon 2020 Research and Innovation Program, under grant agreement No. 871237 (<http://www.project-sophia.eu>),.SOPHIA attempts to contribute to the development of a new generation of HRC technologies which could improve human ergonomics during MMH. The project's technological innovations will allow for improved management of the occupational health challenges posed by WMDs in Europe, which include sick leave, disability, and early job interruption (Van Der Beek et al., 2017; Eurofound, 2015).

2. Materials and Methods

2.1 Participants

Eleven participants (5 females and 6 males; age: 27.73 ± 5.99 years; body mass index [BMI]: 23.06 ± 3.93 kg/m²) took part in the study. The study was carried out at the University of Montpellier in accordance with the Helsinki Declaration and authorized by the University of Montpellier EuroMov's Laboratory Ethics Committee (Protocol number IRB-EM 2103A). Exclusion criteria included inability to give informed written consent, history of musculoskeletal disorders, upper limb, lower limb or trunk surgery, orthopedic or neurological diseases, disorders of the vestibular system, visual impairments or back pain, current pregnancy, current pharmacological treatment, and obesity.

2.2 Inertial Measurement Unit and Electromyographic recordings

The Inertial Measurement Unit (IMU) and Electromyographic (sEMG) data were acquired simultaneously, synchronizing the two systems.

2.2.1 IMU recordings

The Xsens MVN Link system (Xsens, Enschede, The Netherlands) was used to record whole-body kinematics on participants. The MVN Awinda system motion analysis system includes a protocol for measuring whole body kinematics, comprising 17 IMUs placed all over the body to measure the orientation of body segments: 1 on the head, 1 on the sternum, 1 on the pelvis (at the L5/S1 level), and 1 bilaterally on each scapula, upper arm, forearm, hand, thigh, shank, and foot. To achieve proper sensor placement, Xsens MVN whole-body lycra suits in various sizes (M to XXL) were used. Before beginning recordings, the Xsens system was calibrated using the "N-pose and walk" calibration technique for each participant. The Xsens MVN Analyze software (version 2018.0.0) was used to record Xsens data at 60 Hz.

2.2.2. sEMG recordings

The surface myoelectric signals were acquired using a 16-channel Wi-Fi transmission surface electromyograph (FreeEMG300 System, BTS, Milan, Italy) at a sampling rate of 1000 Hz. A Hamming bandpass filter (10-400Hz cut-off frequencies, and a common mode rejection ratio of 100 dB) was used for pre-processing filtering and denoising. Following skin preparation, bipolar Ag/AgCl surface electrodes (diameter 2 cm, H124SG Kendall ARBO, Tyco healthcare, Neustadt/Donau, Germany) were prepared with electroconductive gel and placed over the muscle belly in the direction of the muscle fibers (distance of 2 cm between the centers of the electrodes) in accordance with European recommendations for surface electromyography (Hermens et al., 2000) and the atlas of muscle innervation zones.

Eight bipolar electrodes were placed over the following muscles: anterior deltoideus (AD), posterior deltoideus (PD), biceps brachii caput longum (BBCL), triceps brachii caput longum (TBCL), flexor carpi radialis (FCR), extensor carpi radialis (ECR), rectus abdominis superior (RAS), and erector spinae longissimus (ESL). These muscles were chosen because of their role as flexors and extensors of the shoulder, elbow, wrist, and trunk joints, respectively.

2.3 Experimental procedure

The goal of our experiment was to reproduce an industrial use case proposed by the SME HANKAMP (Netherlands) and shown in Figure 1 (A). The apparatus (shown in Figure 1) consisted of: the BAZAR collaborative robot (only referred to as BAZAR in the following), 4 tables, 1 cylindrical load (5 kilograms) to be displaced and 1 cleaning brush. The task consists in displacing the cylindrical load between the four tables (action which requires lifting, placing and carrying the load) in a predefined order, and cleaning it with the brush (action which requires holding the load in the air with one hand). The experiments are shown in the video available at: <https://youtu.be/vul8iLO0Sdw>.

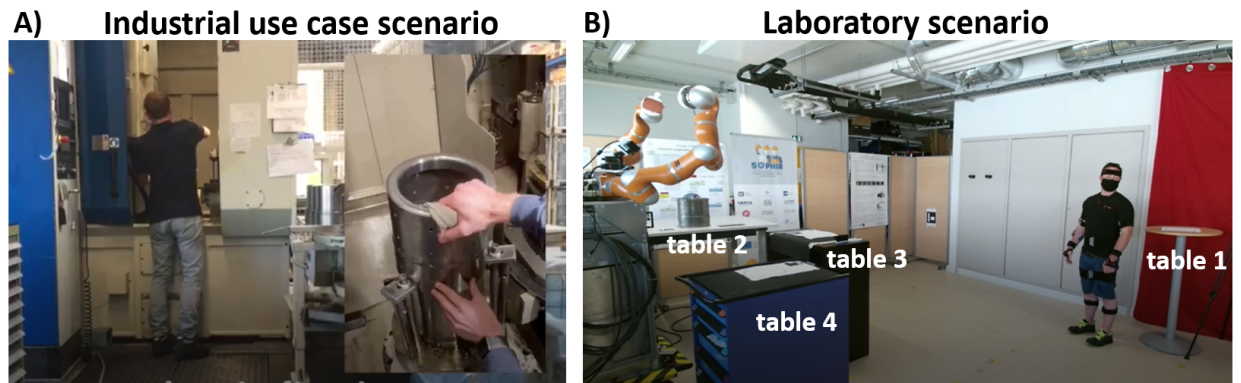


Fig. 1. Industrial use case scenario (A) and laboratory scenario (B).

Each participant completed the task six times: three times without BAZAR and three times with BAZAR. When the task is performed with BAZAR, it eliminates some human activities (lifting, placing and carrying the load). Indeed, it moves the load from table 2 to table 3 (closer to the humans' starting position and at height equal to 100 cm) and from table 3 to table 4 to avoid humans lifting the load from table 2 and 3 respectively. Furthermore, in the brushing phase, BAZAR helps the human, by lifting the load, while he/she brushes it. We randomly ordered the two conditions (with and without BAZAR), for each subject. Before the participant performed either condition for the first time, we instructed him/her by showing a video of the task, and by letting him/her execute it once or until he/she was able to perform it on his/her own, without recording. All subjects performed and completed the task independently the first time without the need to repeat it.

2.3.1 Task without BAZAR

The task without the use of BAZAR can be separated into the following sub-tasks (Figure 2A):

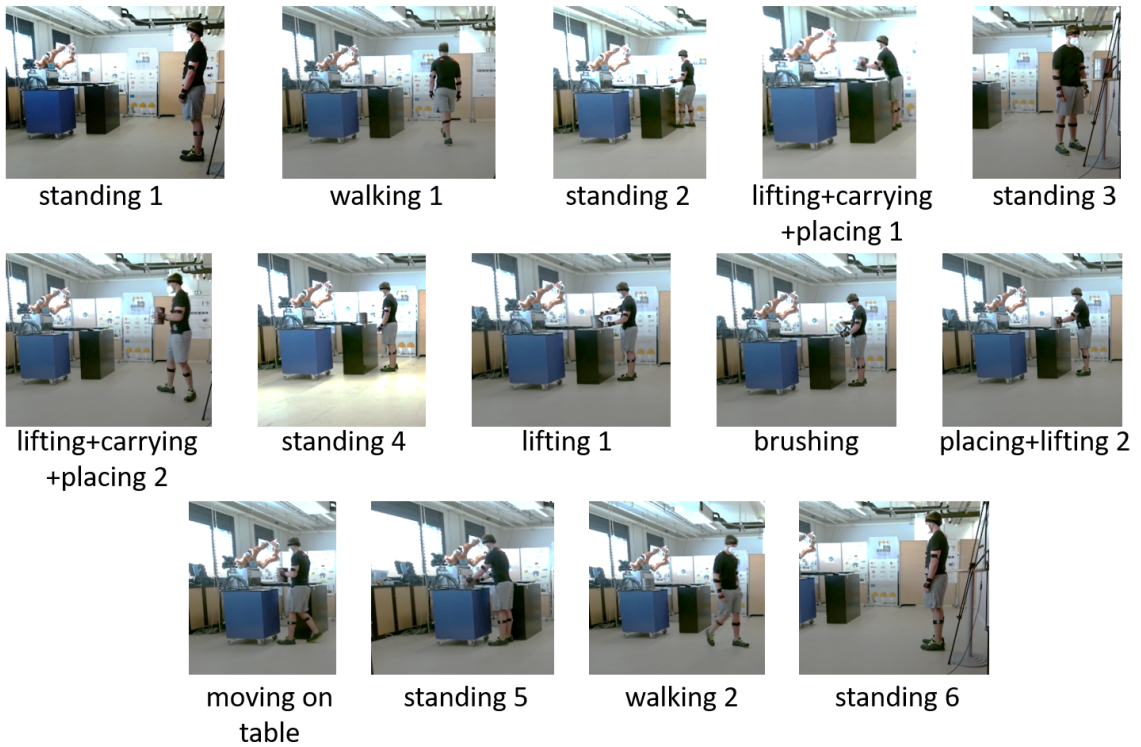
- standing 1: the participant was standing with his/her upper limbs lying along the trunk near table 1;
- walking 1: the participant walked to table 2;
- standing 2: the participant stood in front of table 2 with his/her upper limbs lying along the trunk, while waiting for an acoustic signal;
- lifting+carrying+placing 1: the participant lifted the load from table 2, carried it and placed it on table 1;
- standing 3: the participant stood in front of table 1, with his/her upper limbs lying along the trunk, waiting (approximately 5 seconds) for an acoustic signal;
- lifting+carrying+placing 2: the participant lifted the load, carried it and placed it on table 3;
- standing 4: the participant stood in front of the table 3 with his/her upper limbs lying along the trunk;
- lifting 1: the participant lifted the load and the brush from table 3;
- brushing: the participant cleaned the load with the brush;
- placing +lifting 2: the participant placed the load back on table 3, then lifted it again;
- moving on table: the participant placed the load on table 4;
- standing 5: the participant stood in front of table 4 with his/her upper limbs lying along the trunk;
- walking 2: the participant walked to table 1;
- standing 6: same as static 1.

2.3.2 Task with BAZAR

The task in collaboration with the cobot can be separated into the following sub-tasks (Figure 2B):

- standing 1: the participant stood with his/her upper limbs lying along the trunk in front of table 1
- walking 1: the participant walked to table 3;
- standing 2: the participant stood with his/her upper limbs lying along the trunk in front of table 3, while the robot moved the load from table 2 to table 3;
- lifting+carrying+placing 1: the participant lifted the load from table 3, carried it and placed it on table 1;
- static 3: the participant stood in front of table 1, with his/her upper limbs lying along the trunk, waiting (approximately 5 seconds) for an acoustic signal;
- lifting+carrying+placing 2: the participant lifted, carried and placed the load on table 3;
- standing 4: the participant stood in front of table 3, while the robot lifted the load;
- brushing: while the robot was holding the load, the participant lifted the brush from table 3, and used it to clean the load with his/her left hand;
- placing+walking 2: the participant placed the load on table 3 and walked to table 1 while the robot moved the load to table 4;
- standing 5: same as static 1.

A) Sub-tasks without BAZAR



B) Sub-tasks with BAZAR

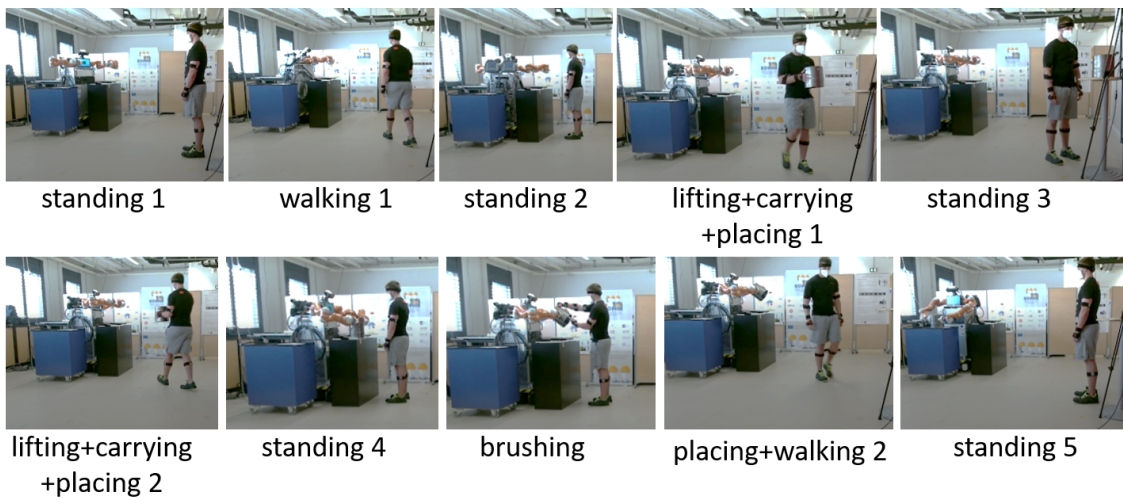


Fig. 2 Sub-tasks of the task without (A) and with (B) BAZAR.

2.3.3 BAZAR description

BAZAR's framework was programmed in C++ within RKCL (Robot Kinematic Control Library, <https://gite.lirmm.fr/rkcl>) (Tarbouriech et al., 2019). The framework was executed on a computer with an Intel(R)

Xeon(R) E5-2620 v3 CPU running Linux with the PREEMPT-RT patch. We used the Fast Research Interface Library (FRI) (<https://cs.stanford.edu/people/tkr/fri/html/>) to communicate with BAZAR’s Kuka arms at 200 Hz.

The framework is composed of:

- a unique kinematic control loop, which sequentially executes the various processes;
- several drivers in charge of exchanging data between each hardware component (e.g., Kuka arms, mobile base, force/torque sensors, camera, etc.) and the controller.

We designed the framework so that distinct hardware components could operate together, even if their control rates are different. This is possible, by parallelizing execution of the kinematic controller and of the components’ communication drivers. Each process runs independently and at varying frequency: the drivers are triggered by the reception of new data coming from the sensors, so that the time rate is fixed for each component. The kinematic control loop time step, instead, is arbitrary and can be freely set by the user. The best performances are obtained when the control loop time step is set equal to the time rate of the fastest driver, so that the driver’s bandwidth is not artificially limited.

In RKCL, each C++ application loads a YAML (<https://yaml.org/>) configuration file at launch time, with the parameters to be used. In this work, the scenario for the whole application is configured as a list of YAML subfiles, each of them defining a robotic *action*. To characterize an action, we specify two frames: the *control frame* to be moved by the robot, and the *reference frame* with respect to which the control frame is moved.

To define the reference frame, in some cases we relied on computer vision and QR codes. We used the Microsoft Kinect V2 RGB-D camera in BAZAR’s head and on the ArUco Library (Garrido-Jurado et al., 2014), which provides real-time marker-based 3D pose estimation.

To generate trajectories between reference frames (i.e., waypoints), we used the Reflexxes Motion Library (Kröger, 2011) with the following parameters: maximum translational velocity=0.5m/s, maximum rotational velocity=0.5 rad/s, maximum translational acceleration=0.2 m/s², and maximum rotational acceleration=0.2 rad/s².

Another fundamental tool, which we used to make the robot safe and compliant, is admittance control (Hogan, 1984). Admittance control deforms the trajectories of each robot hand by passing the forces/torques measured at that hand, through a spring-damper model. The deformation will depend on pre-tuned damping (B) and stiffness (K) gains. These two gains can be tuned differently for forces (which induce deformations along the hand translational degrees of freedom) and torques (which induce deformations along the hand rotational degrees of freedom). By varying the gains, we have designed three admittance control modes: pose, force, and damping control (Tarbouriech et al., 2019), outlined in Table 1.

Degrees of freedom	Translations		Rotations	
Parameter	B (in Ns/m)	K (in N/m)	B (in Ns/rad)	K (in N/rad)
Pose control	150	250	25	40
Damping control	150	0	25	0
Force control	1000	0	500	0

Table 1. Damping (B) and Stiffness (K) gains along the translational and rotational degrees of freedom for pose, damping and force control modes.

In this work, as outlined in 2.3.2 and in Figure 2B, BAZAR had to execute four sub-tasks. We hereby recall the subtasks and specify the actions composing each subtask:

- 1) Moving the load from table 2 to table 3 (during subtask ‘static 2’). Actions: position arms before grasp, grasp load, lift load, turn base, place load, position arms to release load.
- 2) Lifting the load, with the participant standing in front of table 3 (during ‘static 4’). Actions: position arms before grasp, grasp load, lift load.
- 3) Holding the load while the participant brushed it (during ‘brushing’). Action: move load during HRC.
- 4) Moving the load from table 3 to table 4 after the participant finished brushing (during ‘placing+walking 2’). Actions: turn base, place load, position arms to release load.

In summary, the whole experiment relied on the following actions: position arms (e.g., before grasp, to release load), grasp load, turn base, move the load (e.g., place it or lift it, including during HRC). We hereby describe each of these actions.

Position arms: for this action, since the hands are not constrained to one another (i.e., they are not holding anything) we control them independently with pose control. We set a control frame on each hand and use the appropriate QR code as reference frame. The two hands move together towards/away from the load, although each one has a distinct target.

Grasp load: again, we control the hands independently; yet here, we use force control to make the hands move to contact the load – for grasping. Thanks to force control and to the concavities on its hands, BAZAR was able to grasp the load even if its position was not exactly known. In practice, we observed that it could tolerate offsets up to 2 cm from the expected position.

Turn base: when the robot base moves, its proprioception (i.e., the *odometry*) cannot guarantee correct localization. Therefore, we use the ArUco markers to stop the robot when it is facing the load. We placed one marker on each table, at a predefined pose relative to the lifting/placing locations, and asked the participants to place the load at the indicated location after each operation. The control frame is attached to the QR code, and the reference frame is at the mobile base center.

Move load: for this action, we chose the cooperative task representation (Chiacchio et al., 1996). Instead of controlling each arm independently, we considered the robot as a unique entity and described the operations via an absolute task (which controls the motion of the robot in the workspace), and a relative task (which regulates the relative motion between the two hands). As soon as the hands are both in contact with the load, we switch from independent to collaborative control. The grasping and holding of the load is managed by the relative task, which maintains a constant force on the load, while the absolute task moves the load in the workspace. When there is no interaction with the human operator, the absolute task is fully position controlled (i.e. aims at reaching a target pose without considering force measurements), while *during HRC* we controlled the vertical translation and one horizontal rotation degree of freedom in damping mode. By compensating gravity effects (Tarbouriech et al 2019), only the forces applied by the human make the robot move. This allows him/her to move the load with minimal effort.

2.3.4 Isometric maximum voluntary contractions (iMVCs)

To obtain the isometric maximal voluntary contractions (iMVCs), we asked each participant to perform a specific exercise twice with each muscle (Hermens et al., 2000; Barbero et al., 2012; Vera-Garcia et al., 2010).

In more detail, each participant performed the empty can test (Schwartz et al. 2017, Boettcher et al. 2008) for measuring the iMVC of the AD and PD.

Each subject sat comfortably, placed the proximal load of the arm on a table at shoulder height with the shoulder flexed at 90° and an elbow flexion such that the forearm was at 120° from the upper arm, and performed a forearm isometric flexion against resistance for measuring the BBCL iMVC (Farina et al., 1999) and an isometric forearm extension for measuring the TBCL iMVC (Farina et al., 1999).

To acquire the iMVC of the FCR, we asked each participant to sit comfortably, place the forearm on a table with an elbow flexion of around 45°, and perform an isometric hand flexion against resistance (Rota et al., 2013). From the same position, each participant performed an isometric hand extension against resistance for measuring the ECR iMVC (Rota et al., 2013).

Each subject was placed in a supine position and performed an isometric contraction during trunk flexion against resistance, so we could obtain the RAS iMVC, and each subject was placed in a prone position, lying on a mattress, and performed an isometric contraction during trunk extension against resistance, so we could obtain the ESL iMVC (Vera-Garcia et al., 2010).

2.4 Data Analysis

Data were processed using Matlab (version 2018b 9.5.0.1178774, MathWorks, Natick, MA, USA).

2.4.1 Sub-tasks detection

To segment each task in the sub-tasks defined in Sec. 2.3 and shown in Figure 2, we used the vertical velocities of the feet and hands. Figure 3 shows this division in sub-tasks. Starting with the feet velocity signals we conducted a first segmentation, and then we identified the brushing sub-task using the hand velocity signals. This sub-task is the HRC part, which we analyzed in this study to determine the cobot effect on the task. During the task, the IMU and sEMG signals were time-normalized and then interpolated according to the brushing sub-task duration (400 samples) (Ranavolo et al., 2015; Ranavolo et al., 2018; Varrecchia et al., 2021, 2022) [using a linear interpolation procedure to allow a comparison between tasks with different durations.](#)

2.4.2 Bipolar sEMG Processing

To reduce low-frequency artifacts and high-frequency noise, we band-pass filtered the sEMG signals recorded for both iMVC and tasks, with a 3rd order Butterworth filter of bandwidth 25–400 Hz (Butler et al., 2009; Drake and Callaghan, 2006). Then, we filtered the signals with a Notch's filter with cutoff frequency 50Hz, to remove noise due to network signal. The envelope of each task's sEMG signals was then extracted using full-wave rectification and low-pass filtering with a 4th order Butterworth filter at 5 Hz (Winter, 2009). The average iMVC peak value for each muscle has been used to normalize the sEMG envelope (Ranavolo 2021; Burden 2010; Marras and Davis, 2001). The mean ([as the information regarding the overall execution of the task](#)) and maximum ([as a punctual information](#)) values within the brushing sub-task were determined as muscle parameters. [Furthermore, for each muscle we have calculated also the amplitude probability distribution function \(ADPF, Jonsson, 1982\) for the 10, 50, and 90th percentiles. The data from the three repetitions for each condition were averaged for each subject.](#)

2.4.3. Time-Varying Multi-Muscle Coactivation Function (TMCf)

The simultaneous activation (coactivation) of agonist and antagonist muscles is one of the mechanisms adopted by the central nervous system to stabilise the joints or the spine (Granata and Marras, 2000). We used the time-varying multi-muscle coactivation function (TMCf) (Ranavolo et al., 2015) to perform, unlike what is possible with other methods, a time-varying monitoring of the co-activation of more than two muscles without the need for an a-priori classification of the muscles, depending on the generated moment. The TMCf has shown to be particularly useful because it is sensitive to the level of risk and correlated to shear and compression forces in manual lifting activities carried out by a single worker (Ranavolo et al., 2018), as well as in lifting activities shared by multiple workers (Chini et al., 2022). In fatiguing lifting activities (Varrecchia et al., 2022) TMCf is correlated to the local manifestation of muscle fatigue. It was estimated using the following formula:

$$TMCf(d(k), k) = \left(1 - \frac{1}{1 + e^{-12(d(k)-0.5)}}\right) \cdot \frac{(\sum_{m=1}^M sEMG_m(k)/M)^2}{\max_{m=1\dots M} [sEMG_m(k)]}$$

where $d(k)$ is the mean of the differences between the k^{th} samples of each pair of sEMG signals:

$$d(k) = \frac{\sum_{m=1}^{M-1} \sum_{n=m+1}^M |sEMG_m(k) - sEMG_n(k)|}{J(M!/(2!(M-2)!))}$$

In the above equations, J is the length of the signal (400 samples in this case); M is the number of considered muscles; $sEMG_m(k)$ and $sEMG_n(k)$ are the k^{th} sample values of the envelope of the sEMG signals of the m^{th} and n^{th} muscles, respectively.

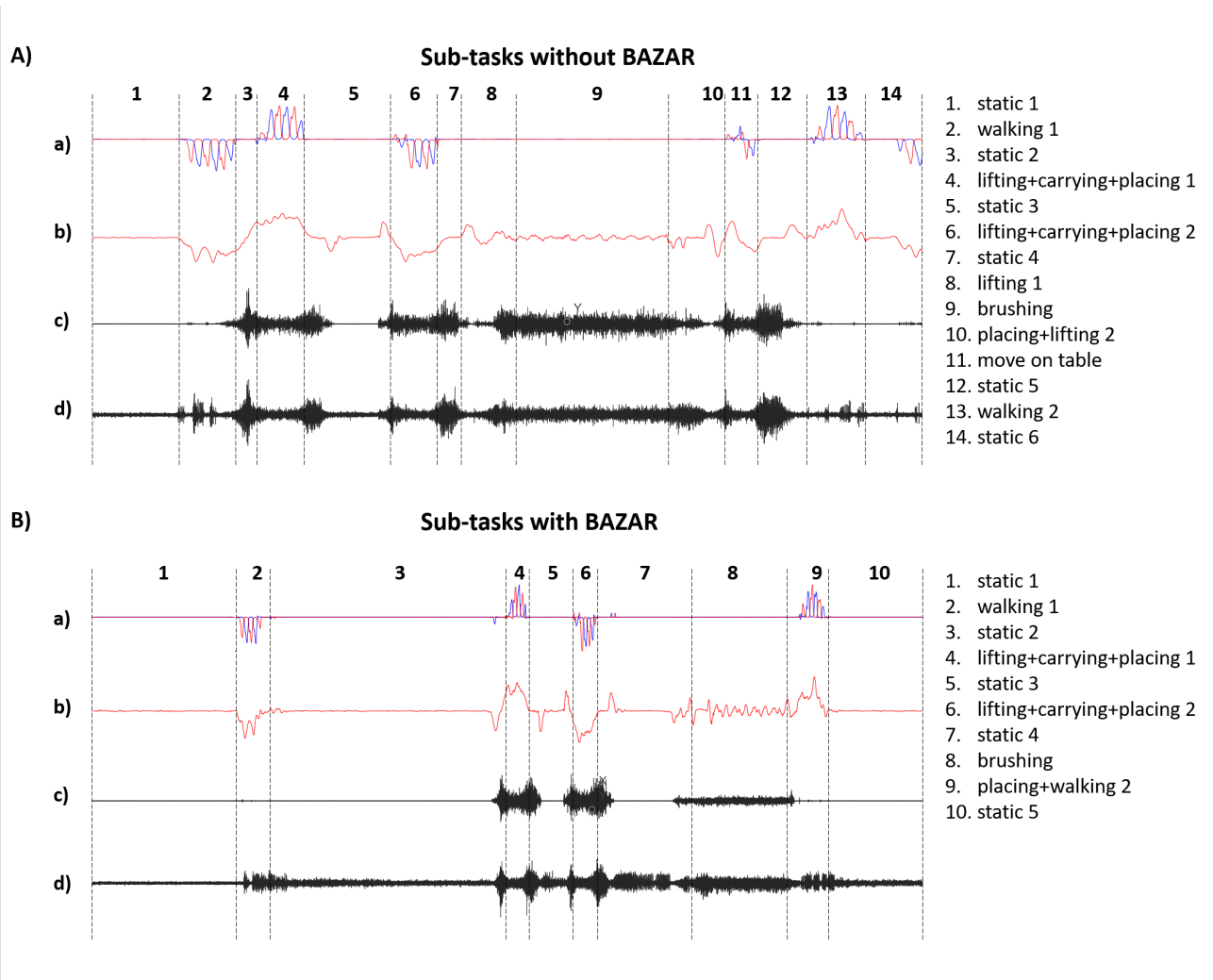


Fig. 3. Vertical velocity of the right (blue) and left (red) foot (a), vertical velocity of the left hand (b), raw sEMG signal for biceps brachii caput longum (c) and raw sEMG signal for triceps brachii caput longum (d) for the task without (A) and with (B) BAZAR. For both tasks, the dashed vertical lines indicate the sub-tasks, which are numbered on the figure and listed in the legend.

TMCf was computed for each antagonistic muscle pair in each joint (shoulder, elbow, wrist, and trunk), for the entire arm, and for all acquired muscles. More in detail, we calculated:

- $TMCf_{AD-PD}$: coactivation of AD and PD muscles, for the shoulder joint;
- $TMCf_{BBCL-TBCL}$: coactivation of BBCL and TBCL muscles, for the elbow joint;
- $TMCf_{FCR-ECR}$: coactivation of FCR and ECR muscles, for the wrist joint;
- $TMCf_{RAS-ESL}$: coactivation of RAS and ESL muscles, for the trunk joint;
- $TMCf_{ARM}$: coactivation of AD, PD, BBCL, TBCL, FCR and ECR muscles, arm coactivation as a whole;
- $TMCf_{ALL}$: coactivation of all acquired muscles, overall coactivation.

For each of the above-mentioned TMCf, we used the mean (for characterizing the overall task execution) and maximum (as a punctual information) values during the brushing sub-task as coactivation indices. Furthermore, for each of the above-mentioned TMCf, we also calculated the ADPF for the 10, 50, and 90th percentiles. The data from the three repetitions for each condition were averaged for each subject.

2.5 Statistical Analysis

To check differences between the two conditions (with and without the cobot), the statistical analysis was carried out using Matlab (version 2018b 9.5.0.1178774, MathWorks, Natick, MA, USA). The Shapiro–Wilk test was used to determine the normality of the data distribution for each parameter. The paired sample t-test or the non-parametric Wilcoxon test (if the data was not normally distributed) was then used to evaluate whether the help of the cobot had determined significant changes in each parameter. The significance level for all statistical analyses was set at p-value < 0.05.

3. Results

For each condition (with and without robot), figures 4, 5 and 6 show the mean and standard deviation of mean values (Figure 4), max values (Figure 5) and ADPF (Figure 6) of each muscle (2nd and 3rd column) and of each evaluated TMCf (1st and 4th column), respectively. Specifically, we reported, for each row in the 2nd and 3rd columns, the values for antagonist muscles and in the 4th column, the corresponding TMCf for each pair of these antagonist muscles. Furthermore, in the first column we reported the values of the TMCf_{ARM} and TMCf_{ALL}.

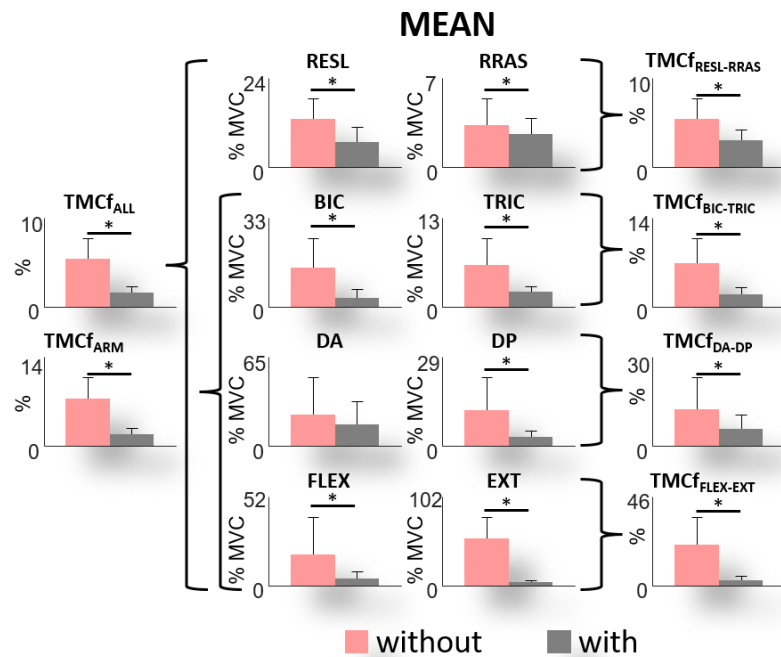


Fig. 4. Mean values (Mean ± SD) of muscles [% MVC] and TMCf [% of coactivation] in both conditions, *without and with* cobot. AD: anterior deltoideus, PD: posterior deltoideus, BBCL: biceps brachii caput longum, TBCL: triceps brachii caput longum, FCR: flexor carpi radialis, ECR: extensor carpi radialis, RAS: rectus abdominis superior, ESL: erector spinae longissimus muscles. TMCf: Time-varying multi-muscle coactivation function. * statistical significance (p < 0.05).

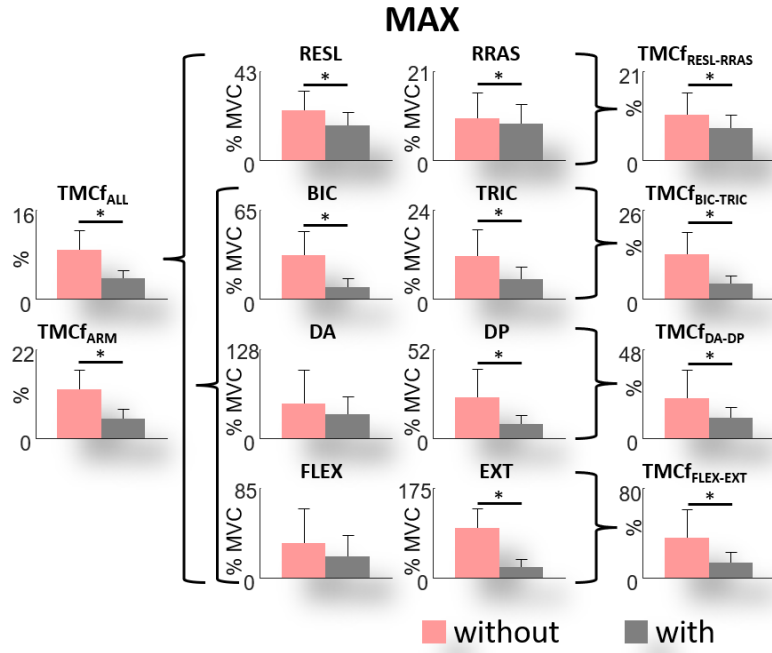


Fig. 5. Max values (Mean \pm SD) of muscle [% MVC] and TMCf [% of coactivation] in both conditions, **without and with BAZAR**. AD: anterior deltoideus, PD: posterior deltoideus, BBCL: biceps brachii caput longum, TBCL: triceps brachii caput longum, FCR: flexor carpi radialis, ECR: extensor carpi radialis, RAS: rectus abdominis superior, ESL: erector spinae longissimus muscles. TMCf: Time-varying multi-muscle coactivation function. * statistical significance ($p < 0.05$).

Considering the mean values (Figure 4), significant effects of the presence of robot for each muscle except for AD and for each evaluated TMCf were found (Table 2): the mean values of muscles and of TMCf significantly decrease when the task is performed with the cobot.

Similarly, considering the max values (Figure 5), for each muscle except for AD and FCR and for each evaluated TMCf, we found significant effects of the presence of the cobot (Table 3): the max values of muscles and of TMCf significantly decrease when the task is performed with the cobot.

		Mean \pm SD	Test Statistics	df	p value	effect size	power
AD	without	23.324 \pm 26.935	$z=-5.333$	9.504	0.594	0.31	0.148
	with	16.038 \pm 16.487					
PD	without	11.669 \pm 10.48	$z=-2.667$	9.504	0.008	0.892	0.736
	with	3.081 \pm 2.012					
BBCL	without	14.594 \pm 10.931	$z=-2.854$	9.504	0.004	1.168	0.923
	with	3.241 \pm 3.261					
TBCL	without	5.959 \pm 3.877	$t=3.249$	10	0.009	1.087	0.9
	with	2.120 \pm 0.844					
FCR	without	18.159 \pm 21.82	$z=-2.934$	9.504	0.003	0.707	0.539
	with	3.957 \pm 4.109					
ECR	without	53.376 \pm 24.896	$t=6.818$	10	<0.001	2.055	0.999
	with	4.150 \pm 2.022					
RAS	without	3.556 \pm 2.183	$z=-2.667$	9.504	0.008	1.454	0.987
	with	2.781 \pm 1.357					
ESL	without	13.171 \pm 5.52	$z=-2.845$	9.504	0.004	1.282	0.96

	with	6.786±4.152						
TMCf_{AD-PD}	without	12.206±10.656	z=-2.223	9.504	0.026	0.708	0.54	
	with	5.664±4.816						
TMCf_{BBCL-TBCL}	without	6.878±3.913	t=4.486	10	0.001	1.404	0.987	
	with	1.989±1.153						
TMCf_{FCR-ECL}	without	21.307±14.159	z=-2.934	9.504	0.003	1.385	0.979	
	with	2.905±1.971						
TMCf_{ESL-RAS}	without	5.382±2.302	z=-2.934	9.504	0.003	1.204	0.936	
	with	2.980±1.229						
TMCf_{ARM}	without	7.510±3.331	t=6.415	10	<0.001	1.91	0.999	
	with	1.845±0.975						
TMCf_{ALL}	without	5.477±2.39	t=6.594	10	<0.001	1.845	0.999	
	with	1.580±0.776						

Table 2. Statistical results of the effect of the cobot on each muscle and TMCf mean values. AD: anterior deltoideus, PD: posterior deltoideus, BBCL: biceps brachii caput longum, TBCL: triceps brachii caput longum, FCR: flexor carpi radialis, ECR: extensor carpi radialis, RAS: rectus abdominis superior, ESL: erector spinae longissimus muscles. TMCf: Time-varying multi-muscle coactivation function. Bold: statistical significance (p<0.05).

		Mean±SD	Test Statistics	df	p value	effect size	power
AD	without	49.541±48.629	z=-0.978	9.504	0.328	0.369	0.19
	with	33.996±26.499					
PD	without	23.584±16.643	t=2.880	10	0.016	1.021	0.862
	with	8.417±4.748					
BBCL	without	32.030±17.844	z=-2.845	9.504	0.004	0.991	0.841
	with	8.559±6.398					
TBCL	without	11.618±7.211	t=2.338	10	0.041	0.991	0.841
	with	5.420±3.246					
FCR	without	32.146±33.531	z=-1.956	9.504	0.051	0.417	0.23
	with	19.936±20.505					
ECR	without	96.659±38.115	z=-2.934	9.504	0.003	2.276	0.999
	with	20.852±14.658					
RAS	without	9.921±5.94	t=2.995	10	0.013	0.255	0.12
	with	8.547±4.59					
ESL	without	23.863±9.57	z=-2.490	9.504	0.013	0.835	0.68
	with	16.852±6.136					
TMCf_{AD-PD}	without	21.482±15.484	z=-2.134	9.504	0.033	0.771	0.611
	with	11.037±5.775					
TMCf_{BBCL-TBCL}	without	13.011±6.666	t=3.732	10	0.004	1.419	0.988
	with	4.633±2.091					
TMCf_{FCR-ECL}	without	35.840±25.587	z=-2.934	9.504	0.003	1.019	0.841
	with	13.063±9.921					
TMCf_{ESL-RAS}	without	10.643±5.222	t=4.016	10	0.002	0.669	0.518
	with	7.597±3.119					

TMCf_{ARM}	without	12.184±4.672	t=4.721	10	0.001	1.792	0.999
	with	4.931±2.256					
TMCf_{ALL}	without	8.906±3.505	t=5.213	10	<0.001	1.719	0.999
	with	3.675±1.549					

Table 3. Statistical results of the effect of the cobot on each muscle and TMCf max values. AD: anterior deltoideus, PD: posterior deltoideus, BBCL: biceps brachii caput longum, TBCL: triceps brachii caput longum, FCR: flexor carpi radialis, ECR: extensor carpi radialis, RAS: rectus abdominis superior, ESL: erector spinae longissimus muscles. TMCf: Time-varying multi-muscle coactivation function. Bold: statistical significance ($p < 0.05$).

The 10th, 50th and 90th percentiles of ADPFs are reported in Table 4. Considering the 10th percentile (first dotted horizontal line in each plot of Figure 6), significant effects of the presence of cobot for each muscle (AD: $p=0.001$, PD: $p=0.001$, BBCL: $p=0.005$, TBCL: $p=0.002$, FCR: $p=0.001$, ECR: $p < 0.001$, RAS: $p=0.025$ and ESL: $p=0.001$) and for each evaluated TMCf (TMCf_{AD-PD}: $p=0.001$, TMCf_{BBCL-TBCL}: $p < 0.001$, TMCf_{FCR-ECR}: $p=0.001$, TMCf_{RAS-ESL}: $p=0.001$, TMCf_{ARM}: $p < 0.001$ and TMCf_{ALL}: $p=0.001$) were found: the mean values of ADPF of muscles and of TMCf significantly decrease when the task is performed with the cobot. Considering the 50th percentile (second dotted horizontal line in each plot of Figure 6), significant effects of the presence of cobot for FCR ($p=0.007$) and ECR ($p=0.013$) muscles and for TMCf_{FCR-ECR} ($p=0.005$), TMCf_{ARM} ($p=0.010$) and TMCf_{ALL} ($p=0.010$) were found: the 50th percentile of ADPF of these muscles and of TMCf significantly decrease when the task is performed with the cobot. Considering the 90th percentile (first dotted horizontal line in each plot of Figure 6), significant effects of the presence of cobot for BBCL ($p=0.001$), TBCL ($p=0.027$) and ESL ($p=0.002$) muscles and for TMCf_{BBCL-TBCL} ($p=0.003$), TMCf_{ARM} ($p=0.008$) and TMCf_{ALL} ($p=0.002$) were found: the mean values of ADPF of these muscles and of TMCf significantly increase when the task is performed with the cobot.

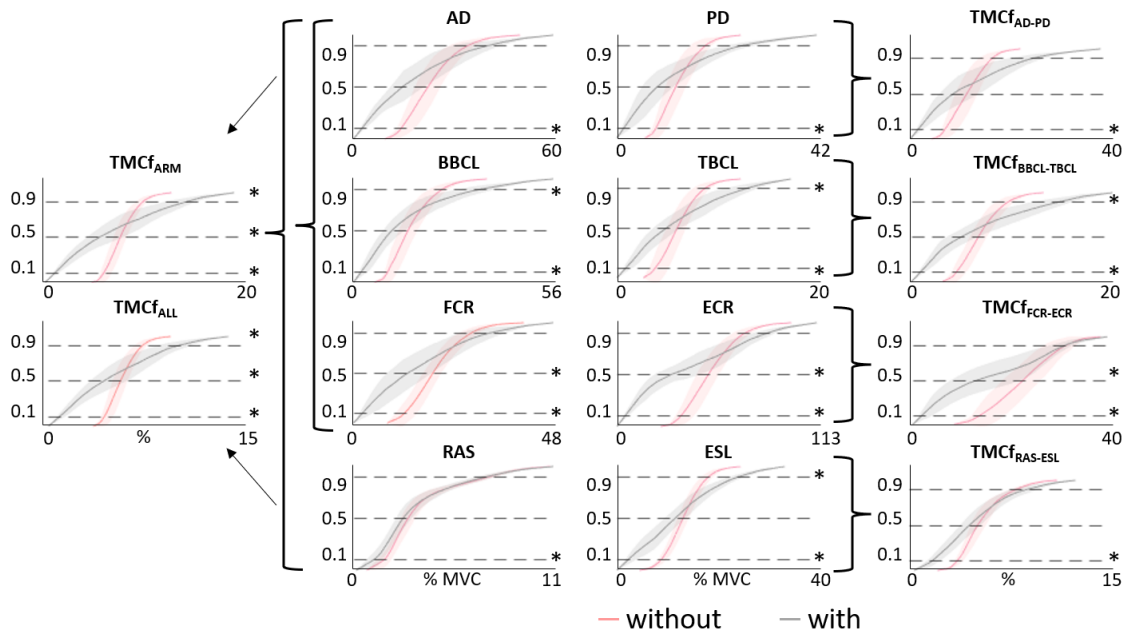


Fig. 6. Mean values (Mean \pm SD) of amplitude probability distribution function (APDF) with the 10, 50, and 90th percentiles in both conditions, without and with cobot. AD: anterior deltoideus, PD: posterior deltoideus, BBCL: biceps brachii caput longum, TBCL: triceps brachii caput longum, FCR: flexor carpi radialis, ECR: extensor carpi radialis, RAS: rectus abdominis superior, ESL: erector spinae longissimus muscles. TMCf: Time-varying multi-muscle coactivation function. * statistical significance ($p < 0.05$).

		10 th	50 th	90 th
AD	without	15.795±20.496	22.686±26.843	31.658±35.245
	with	2.546±1.757	17.210±16.611	37.141±29.583
PD	without	8.523±8.509	12.41±11.375	17.274±14.478
	with	1.489±1.127	7.951±4.841	25.983±17.118
BBCL	without	9.241±7.828	13.777±10.525	20.467±14.575
	with	1.733±1.020	11.434±8.51	33.436±18.595
TBCL	without	4.125±2.548	5.720±3.699	7.993±5.494
	with	0.937±0.498	4.739±3.009	12.068±6.877
FCR	without	13.365±17.217	18.673±23.908	26.713±34.577
	with	2.272±2.284	12.487±	28.522±35.095
ECR	without	38.227±19.744	51.69±24.621	69.798±30.01
	with	4.263±1.93	31.39±15.827	81.047±37.503
RAS	without	1.672±1.264	2.843±1.844	7.101±4.387
	with	1.156±0.767	2.618±1.435	6.835±3.755
ESL	without	8.944±4.72	13.00±5.413	17.245±6.887
	with	2.480±1.211	11.390±4.967	22.714±9.924
TMCf_{AD-PD}	without	8.876±8.486	12.003±10.699	15.689±12.923
	with	1.512±0.922	8.68±5.724	21.125±12.371
TMCf_{BBCL-TBCL}	without	4.908±2.893	6.636±3.863	9.026±5.055
	with	0.873±0.347	5.387±3.188	14.214±6.702
TMCf_{FCR-ECL}	without	14.991±10.151	21.022±14.095	27.649±18.704
	with	1.930±1.071	13.089±8.966	26.229±14.275
TMCf_{ESL-RAS}	without	3.599±1.652	5.012±2.084	7.855±3.624
	with	1.789±0.676	4.514±1.934	8.433±3.559
TMCf_{ARM}	without	5.978±2.774	7.336±3.349	9.161±3.839
	with	0.935±0.381	5.383±2.018	12.097±4.287
TMCf_{ALL}	without	4.377±1.983	5.366±2.389	6.639±2.82
	with	0.825±0.349	4.111±1.447	8.775±3.042

Table 4. Amplitude probability distribution function (APDF) at the 10th, 50th, and 90th percentiles (Mean ± SD) of muscle [% MVC] and TMCf [% of coactivation] in both conditions, without and with BAZAR. AD: anterior deltoideus, PD: posterior deltoideus, BBCL: biceps brachii caput longum, TBCL: triceps brachii caput longum, FCR: flexor carpi radialis, ECR: extensor carpi radialis, RAS: rectus abdominis superior, ESL: erector spinae longissimus muscles. TMCf: Time-varying multi-muscle coactivation function. * statistical significance ($p < 0.05$).

4. Discussion

In this work, we investigated a hybrid worker-robot MMH, throughout the execution of a real-world use case, extrapolated and recreated from an industrial context, to examine the changes of worker motor coordination and physical effort. In detail, we examined upper limb coactivation and muscle activation while doing the task with and without the dual-arm mobile cobot BAZAR, to see how BAZAR could help improve coordination.

Overall, our findings suggest that using BAZAR to perform the specific MMH improves coordination and reduces the workers' physical effort as compared to performing the identical task without BAZAR. In particular, there is a reduction in both upper limb co-activation and muscle activation (Fig. 4 and 5, Table 2 and 3).

The confirmation of our hypothesis shows that the worker executes the task with less physical effort and improved motor coordination throughout the subphases of the work cycle where there is true collaboration between this bimanual collaborative robot and the worker. This suggests that the deployment of cobots will represent innovative ergonomic interventions for reducing the occurrence of WMDs in the industrial setting. This could have a positive impact on employee absences, moves and early work interruption.

The TMCf was significantly lower in each antagonistic muscle pair of the shoulder, elbow, wrist, and trunk joints and for the entire arm and for all acquired muscles. This reduction was highlighted by taking into account not only the mean value (Fig. 4, Table 2) (Ranavolo 2021), which expresses what happens throughout the task and provides information on the task's overall execution, but also the maximum value (Fig. 5, Table 3) (Ranavolo 2021), which is a punctual index that provides information on the maximum value of simultaneous antagonist muscle activation during the task. These findings on muscle joint co-activation show that designing a hybrid worker-robot MMH promotes a significant reduction in antagonist muscle activations and in counteracting agonist actions, lowering moments that do not contribute to the needed net joint moments (Childs et al., 2004; Collins et al., 2011; Griffin and Guilak, 2005; Lewek et al., 2004). Compressive loading across the joints is also reduced as a result of the reduced muscle co-activation (Granata and Marras, 1995, 2000; Marras and Granata 1996; Marras and Mirka, 1993; Ranavolo et al., 2015, 2018b). Finally, lower co-activation of upper-limb and trunk muscles results in more functionally advantageous and efficient motions, by lowering physiological and metabolic costs, resulting in power growth (Franchi et al 2017).

Considering the muscular activity of upper limb, a significant reduction is shown for each investigated muscle except for the mean (Fig. 4, Table 2) and maximum (Fig. 5, Table 3) values of anterior deltoideus muscle (which is a shoulder flexor muscle) and for the maximum value of flexor carpi radialis muscle (which is a wrist flexors muscle). These results could be due to a high variability of activation of these muscles also caused by a different posture and maintenance of the object for the participants, during the execution of the task without BAZAR.

The APDF (Figure 6) shows the trend of muscular activities in % MVC and of % of coactivation. When BAZAR collaborates with subjects the mean values of 10th percentile are lower respect to the condition without BAZAR for each muscle (Figure 6 and Table 4). The ADPFs increase more slowly when subjects perform the task without BAZAR with the initial muscle activities always higher with respect to the condition with BAZAR. Furthermore, when BAZAR helps the subjects, the mean values of 10th percentile never exceeded the limits (5 % MVC) of acceptable muscular load for the static load level (10th) that were found in studies of muscular endurance during dynamic work (Jonsson, 1982). Additionally, with the exception of the AD and ECR muscles, the mean values of the median (50th percentile) load level are lower when BAZAR is used (Fig. 6 and Table 4), and they never go over the limit for static load levels (14%, Jonsson, 1982). Furthermore, the peak loads (90th percentile) do not exceed the limit (70%) in both conditions with and without BAZAR.

The results of this study show that the HRC technologies which share the workers' workspace, not only offload them from external loads and improve efficiency and quality of the task execution; they also allow a reduction of the worker physical effort when s/he physically interacts with the robot, since the latter affects the worker's physiological motor strategy.

Indeed, "The experimental session involved the implementation of a hybrid scenario in which a human and a robot collaborate. In addition to subphases when the cobot replaces the worker, there is a subphase where worker and cobot

interact physically. In this subphase, according to our findings, the worker's physical effort is reduced (a rather obvious effect), but it also enables the worker to use a more coordinated motor strategy. As a result, giving a load to the machine improves coordination, rather than reducing it, and enables the worker to cooperate and coordinate with the robot partner.

4.1 Limitation and future developments

The small sample size (11 subjects) is a limitation of the study due to the fact that the experimental session was very complex and long since it involved performing the work task twice, without and with the BAZAR robot. Furthermore, the experiments were possible only during a limited time period, when two research groups could work together at the University of Montpellier, sharing their knowledge and technologies within the European Union's Horizon 2020 SOPHIA project (please see the “funding” section). Future studies should include larger sample sizes, useful for confirming the results of this study, and we will include subjective information collected through the administration of questionnaires related to usability and acceptability of the cobot by the worker. Furthermore, future experimental sessions should include subjective effort indicators such as subjective workload (e.g., NASA Task Load Index, Hart & Staveland, 1988) or ratings of perceived exertion (e.g., fatigue scale, Borg et al. 1982). We should also verify whether these subjective indicators are correlated to the objective measures presented in this article.

Furthermore, in this study, BAZAR moves in the space interacting with the worker thanks to the presence of QR codes. This could be considered as a limitation of the study. A future development could include the use of a robot that supports the *suitability for individualization* that is the possibility of adapting to the needs and abilities of the worker (Ajoudani et al., 2020). Indeed, the new opportunity represented by the fourth industrial revolution is allowing the design of flexible and reconfigurable hybrid work environments, thanks to the use of innovative wearable sensors for monitoring and feedback (e.g. haptic stimuli to specific areas of the body). Exoskeletons and cobots embed new instrumental-based tools (i.e. myoelectric interfaces which monitor muscle activation amplitude and fatigue), with advanced interaction and sensing capabilities. These tools can evaluate the workers' physical states, assess their effectiveness on motor performance, respond to their intentions in a timely manner and offload them from internal loadings (Lotti et al., 2020; Ajoudani et al., 2020; Kapelner et al., 2019, 2020; Lobov et al., 2018; Roche et al., 2014; Hahne et al., 2014; Gordon et al., 2013; Kiguchi et al., 2012). In future work, BAZAR could be controlled by using kinematic, kinetic and sEMG-based signals acquired from workers through an effective interaction between humans and robots, that ensures a correct information exchange between natural and artificial side. Indeed, only these suitable interfaces can monitor human behavior to properly plan the execution of the collaborative task and can allow mutual awareness of the human–robot dyad (Ajoudani et al., 2020).

Funding: The research presented in this article was carried out as part of the SOPHIA project, which has received funding from the European Union's Horizon 2020 research and innovation programme under Grant Agreement No. 871237.

Acknowledgments: We are extremely grateful to Freek Tonis and Pim Siahaya from HANKAMP for their help with the experimental procedure.

Disclosure statement: The authors report there are no competing interests to declare.

Availability of data: The data that support the findings of this study are openly available in https://gite.lirmm.fr/humar/research-projects/sophia_dataset_example.

Figures: caption and alt text

Figure 1 Caption: Industrial use case scenario (A) and laboratory scenario (B).

Figure 1 Alt Text: Industrial use case scenario proposed by the SME HANKAMP (Netherlands) is shown in the panel A while in the panel B the laboratory scenario is shown: it consisted of the BAZAR collaborative robot (only referred to as BAZAR in the following), 4 tables, 1 cylindrical load (5 kilograms) to be displaced and 1 cleaning brush.

Figure 2 Caption: Sub-tasks of the task without (A) and with (B) BAZAR.

Figure 2 Alt Text: In the panel A the sub-tasks of the task without BAZAR are shown: standing 1; walking 1; standing 2; lifting+carrying+placing 1; standing 3; lifting+carrying+placing 2; standing 4; lifting 1; brushing; placing +lifting 2; moving on table; standing 5; walking 2; standing 6. In the panel B the sub-tasks of the task with BAZAR are shown: standing 1; walking 1; standing 2; lifting+carrying+placing 1; lifting+carrying+placing 2; standing 4; brushing; placing+walking 2; standing 5.

Figure 3 Caption: Vertical velocity of the right (blue) and left (red) foot (a), vertical velocity of the left hand (b), raw sEMG signal for biceps brachii caput longum (c) and raw sEMG signal for triceps brachii caput longum (d) for the task without (A) and with (B) BAZAR. For both tasks, the dashed vertical lines indicate the sub-tasks, which are numbered on the figure and listed in the legend.

Figure 3 Alt Text: Panel A shows the vertical velocity of the right (blue) and left (red) foot, the vertical velocity of the left hand, the raw sEMG signal for biceps brachii caput longum and raw sEMG signal for triceps brachii caput longum for the task without BAZAR. In each plot there are dashed vertical lines indicating the sub-tasks (standing 1; walking 1; standing 2; lifting+carrying+placing 1; standing 3; lifting+carrying+placing 2; standing 4; lifting 1; brushing; placing +lifting 2; moving on table; standing 5; walking 2; standing 6), which are numbered on the figure and listed in the legend. Panel B shows the same data referring to the task with BAZAR (sub-tasks: standing 1; walking 1; standing 2; lifting+carrying+placing 1; lifting+carrying+placing 2; standing 4; brushing; placing+walking 2; standing 5).

Figure 4 Caption: Mean values (Mean \pm SD) of muscles [% MVC] and TMCf [% of coactivation] in both conditions, without and with cobot. AD: anterior deltoideus, PD: posterior deltoideus, BBCL: biceps brachii caput longum, TBCL: triceps brachii caput longum, FCR: flexor carpi radialis, ECR: extensor carpi radialis, RAS: rectus abdominis superior, ESL: erector spinae longissimus muscles. TMCf: Time-varying multi-muscle coactivation function. * statistical significance ($p < 0.05$).

Figure 4 Alt Text: A bar plot of Mean values (Mean \pm SD) of each acquired muscles [% MVC] and each evaluated Time-varying multi-muscle coactivation function [% of coactivation] in both conditions, without and with cobot are shown in the figure. TMCf: Time-varying multi-muscle coactivation function. The figure shows statistical significance reported in the text with an asterisk.

Figure 5 Caption: Max values (Mean \pm SD) of muscles [% MVC] and TMCf [% of coactivation] in both conditions, without and with cobot. AD: anterior deltoideus, PD: posterior deltoideus, BBCL: biceps brachii caput longum, TBCL: triceps brachii caput longum, FCR: flexor carpi radialis, ECR: extensor carpi radialis, RAS: rectus abdominis superior, ESL: erector spinae longissimus muscles. TMCf: Time-varying multi-muscle coactivation function. * statistical significance ($p < 0.05$).

Figure 5 Alt Text: A bar plot of Max values (Mean \pm SD) of each acquired muscles [% MVC] and each evaluated Time-varying multi-muscle coactivation function [% of coactivation] in both conditions, without and with cobot are shown in the figure. TMCf: Time-varying multi-muscle coactivation function. The figure shows statistical significance reported in the text with an asterisk.

Figure 6 Caption: Mean values (Mean \pm SD) of amplitude probability distribution function (APDF) with the 10, 50, and 90th percentiles in both conditions, without and with cobot. AD: anterior deltoideus, PD: posterior deltoideus, BBCL: biceps brachii caput longum, TBCL: triceps brachii caput longum, FCR: flexor carpi radialis, ECR: extensor carpi radialis, RAS: rectus abdominis superior, ESL: erector spinae longissimus muscles. TMCf: Time-varying multi-muscle coactivation function. * statistical significance ($p < 0.05$).

Figure 6 Alt Text: Figure shows the Mean values (Mean \pm SD) of amplitude probability distribution function (APDF) with the 10, 50, and 90th percentiles in both conditions, without and with cobot. The APDF are shown for each acquired muscles [% MVC] and each evaluated Time-varying multi-muscle coactivation function.

References

1. Ajoudani, A.; Albrecht, P.; Bianchi, M.; Cherubini, A.; Del Ferraro, S.; Fraisse, P.; Fritzsche, L.; Garabini, M.; Ranavolo, A.; Rosen, P.H.; Sartori, M.; Tsagarakis, N.; Vanderborght, B.; Wischniewski, S. Smart collaborative systems for enabling flexible and ergonomic work practices [industry activities]. *IEEE Robot. Autom. Mag.* **2020**, *27*, 169–176.
2. Alberto, R.; Draicchio, F.; Varrecchia, T.; Silvetti, A.; Iavicoli, S. Wearable Monitoring Devices for Biomechanical Risk Assessment at Work: Current Status and Future Challenges-A Systematic Review. *Int J Environ Res Public Health*. **2018** Sep 13, *15(9)*, 2001. doi: 10.3390/ijerph15092001. Erratum in: *Int J Environ Res Public Health*. 2018 Nov 16; *15(11)*: PMID: 30217079; PMCID: PMC6163390.
3. Anton, D.; Mizner, R. L.; Hess, J. A. The effect of lift teams on kinematics and muscle activity of the upper extremity and trunk in bricklayers. *J Orthop Sports Phys Ther.* **2013**, *43(4)*, 232-241.
4. Baltrusch S. J.; Krause, F.; de Vries, A.W.; van Dijk, W.; de Looze, M.P. What about the human in human robot collaboration? *Ergonomics*. **2021** Oct 13, 1-22. doi: 10.1080/00140139.2021.1984585.
5. Barbero, M., Merletti, R., Rainoldi, A. Atlas of Muscle Innervation Zones: Understanding Surface Electromyography and its Applications. Springer, New York. **2012**. <http://doi:10.1007/978-88-470-2463-2>.
6. Barrett, R. S.; Dennis, G. J. Ergonomic issues in team lifting. *Hum Factors Ergon Manuf.* **2005**, *15(3)*, 293-307.
7. Behrens, R.; Saenz, J.; Vogel, C., Elkmann N. Upcoming Technologies and Fundamentals for Safeguarding All Forms of Human-Robot Collaboration. *8th Int. Conf. Saf. Ind. Autom. Syst.* **2015** November, *18-20*, 18–23.
8. Boettcher, C.E.; Ginn, K.A.; Cathers, I. Standard maximum isometric voluntary contraction tests for normalizing shoulder muscle EMG. *J Orthop Res.* **2008** Dec, *26(12)*, 1591-7. doi: 10.1002/jor.20675. PMID: 18528827.
9. Borg, G.A. Psychophysical bases of perceived exertion. *Med. Sci. Sports Exerc.* **1982**, *14*, 377–381.
10. Brookham, R. L., Middlebrook, E. E., Grewal, T. J., Dickerson, C. R. The Utility of an Empirically Derived Co-activation Ratio for Muscle Force Prediction Through Optimization. *J Biomech.* **2011**, *44 (8)*, 1582–1587.
11. Burden, A. How should we normalize electromyograms obtained from healthy participants? What we have learned from over 25 years of research. *J Electromyogr Kinesiol.* **2010**, *20*, 1023–1035.
12. Butler, H.L.; Newell, R.; Hubley-Kozey, C.L.; Kozey, J.W. The Interpretation of Abdominal Wall Muscle Recruitment Strategies Change when the Electrocardiogram (ECG) is Removed from the Electromyogram (EMG). *J Electromyogr Kinesiol.* **2009**, *19(2)*, 102–113. <http://doi:10.1016/j.jelekin.2007.10.004>.
13. Cherubini, A.; Passama, R.; Navarro, B.; Sorour, M.; Khelloufi, A.; Mazhar, O.; Tarbouriech, S.; Zhu, J.; Tempier, O.; Crosnier, A.; Fraisse, P.; Ramdani, S. A collaborative robot for the factory of the future: BAZAR. *J Adv Manuf Technol.* **2019**, *105 (9)*, 3643-3659.
14. Chiacchio, P.; Chiaverini, S.; Siciliano, B. Direct and inverse kinematics for coordinated motion tasks of a two-manipulator system. *J Dyn Syst Meas Control.* **1996**, *118 (4)*, 691–697.
15. Childs, J. D.; Sparto, P. J.; Fitzgerald, G. K.; Bizzini, M.; Irrgang, J. J. Alterations in Lower Extremity Movement and Muscle Activation Patterns in Individuals with Knee Osteoarthritis. *Clin Biomech (Bristol, Avon).* **2004**, *19(1)*, 44–49.
16. Chini, G.; Varrecchia, T.; Tatarelli, A.; Silvetti, A.; Fiori, L.; Draicchio, F.; Ranavolo, A. Trunk muscle co-activation and activity in one-and two-person lifting. *Int J Ind Ergon.* **2022**, *89*, 103297.
17. Collins, A.; Blackburn, J. T.; Olcott, C.; Yu, B.; Weinhold, P. The Impact of Stochastic Resonance Electrical Stimulation and Knee Sleeve on Impulsive Loading and Muscle Co-contraction During Gait in Knee Osteoarthritis. *Clin Biomech (Bristol, Avon).* **2011**, *26 (8)*, 853–858.
18. Dennis, G.J.; Barrett, R.S. Spinal loads during individual and team lifting. *Ergonomics*. **2002**, *45(10)*, 671– 681.

19. Dennis, G.J.; Barrett, R.S. Spinal loads during two-person team lifting: Effect of matched versus unmatched standing height. *Int J Ind Ergon.* **2003a**, *32*(1), 25–38.
20. Dennis, G.J.; Barrett, R.S. Spinal loads during two-person team lifting: Effect of load mass distribution. *Int J Ind Ergon.* **2003b**, *32*(5), 349–358.
21. Drake, J.D.; Callaghan, J.P. Elimination of electrocardiogram contamination from electromyogram signals: An evaluation of currently used removal techniques. *J Electromyogr Kinesiol.* **2006**, *16* (2), 175-187.
22. El Makrini, I.; Elprama, S. A.; Van den Bergh, J.; Vanderborght, B.; Knevels, A. J.; Jewell, C. I.; Stals, F.; De Coppel, G.; Ravyse, I.; Potargent, J.; Berte, J.; Diericx, B.; Waegeman, T.; Jacobs, A. Working with walt: How a cobot was developed and inserted on an auto assembly line. *IEEE Robotics & Automation Magazine.* **2018**, *25*(2), 51-58.
23. Elprama, S. A.; Jewell, C. I. C. Jacobs, A., El Makrini, I., Vanderborght, B. Attitudes of factory workers towards industrial and collaborative robots. *Conference on Human-Robot Interaction (HRI 2017).* **2017**, 113 - 114. doi:10.1145/3029798.3038309.
24. Eurofound. European Working Conditions Survey 2015; Eurofound: Brussels, Belgium, **2019**. Available online: <https://www.eurofound.europa.eu/data/european-working-conditions-survey> (accessed on 04 May 2022).
25. Faber, G.; Visser, S.; Van der Molen, H. F.; Kuijper, P. P. F. M.; Hoozemans, M. J.; Van Dieën, J. H.; Frings-Dresen, M. H. Does team lifting increase the variability in peak lumbar compression in ironworkers? *Work*, **2012**, *41*(Supplement 1), 4171-4173.
26. Farina, D.; Merletti, R.; Rainoldi, A.; Buonocore, M.; Casale, R. Two methods for the measurement of voluntary contraction torque in the biceps brachii muscle. *Med Eng Phys.* **1999** Oct, *21*(8), 533-40. doi: 10.1016/s1350-4533(99)00076-4. PMID: 10672786.
27. Franchi, M. V.; Reeves, N. D.; Narici, M. V. Skeletal Muscle Remodeling in Response to Eccentric vs. Concentric Loading: Morphological, Molecular, and Metabolic Adaptations. *Front Physiol.* **2017**, *8*, 447. <https://doi.org/10.3389/fphys.2017.00447>
28. Garrido-Jurado, S.; Muñoz-Salinas, R.; Madrid-Cuevas, F. J.; Marín-Jiménez, M. J. Automatic generation and detection of highly reliable fiducial markers under occlusion. *Pattern Recognit.* **2014**, *47*(6), 2280-2292.
29. Gordon, K.E.; Kinnaird, C.R.; Ferris, D.P. Locomotor adaptation to a soleus EMG-controlled antagonistic exoskeleton. *J Neurophysiol.* **2013**, *109*, 1804– 14. doi: 10.1152/jn.01128.2011
30. Granata, K. P.; Marras, W. S. Cost-Benefit of Muscle Cocontraction in Protecting Against Spinal Instability. *Spine (Phila Pa 1976).* **2000**, *25* (11): 1398–1404.
31. Granata, K.P.; Marras, W.S. The influence of trunk muscle coactivity on dynamic spinal loads. *Spine.* **1995**, *20* (8), 913–919. <https://doi.org/10.1097/00007632-199504150-00006>.
32. Griffin, T.; F. Guilak. The Role of Mechanical Loading in the Onset and Progression of Osteoarthritis. *Exerc Sport Sci Rev.* **2005**, *33* (4), 195–200.
33. Hahne, J.M.; Biessmann, F.; Jiang, N.; Rehbaum, H.; Farina, D.; Meinecke, F.C.; Müller, K.R.; Parra, L.C. Linear and nonlinear regression techniques for simultaneous and proportional myoelectric control. *IEEE Trans Neural Syst Rehabil Eng.* **2014**, *22*, 269–79. doi: 10.1109/TNSRE.2014.2305520
34. Hart, S. G., Staveland, L. E. Development of NASA-TLX (Task Load Index): Results of empirical and theoretical research. In P. A. Hancock & N. Meshkati (Eds.), *Human mental workload. North-Holland.* **1988**, 139–183. [https://doi.org/10.1016/S0166-4115\(08\)62386-9](https://doi.org/10.1016/S0166-4115(08)62386-9).
35. Hermens, H.J.; Freriks, B.; Disselhorst-Klug, C.; Rau, G. Development of recommendations for SEMG sensors and sensor placement procedures. *J Electromyogr Kinesiol.* **2000**, *10*, 361–374.
36. Hogan, N. "Impedance control: An approach to manipulation." *1984 American control conference.* IEEE, 1984.
37. ISO/DIS 11228-1. Ergonomics—Manual Handling—Part 1: Lifting and Carrying; ISO: Geneva, Switzerland, **2003**.
38. Ito, H.; Yamamoto, K.; Mori, H.; Ogata, T. Efficient multitask learning with an embodied predictive model for door opening and entry with whole-body control. *Sci. Robot.* **2022**, *7*(65), eaax8177.
39. Jonsson, B. Measurement and evaluation of local muscular strain in the shoulder during constrained work. *J. Hum. Ergol.* **1982**, *11*(1), 73–88.
40. Kapelner, T.; Sartori, M.; Negro, F., Farina, D. Neuro-Musculoskeletal Mapping for Man-Machine *Interfacing.* *Sci Rep.* **2020**, *10*, 5834.
41. Kapelner, T.; Vujaklija, I.; Jiang, N.; Negro, F.; Aszmann, O.C.; Principe, J.; Farina, D. Predicting wrist kinematics from motor unit discharge timings for the control of active prosthesis. *J Neuroeng Rehabil.* **2019**; *16*, 47.
42. Kiguchi, K.; Hayashi, Y. An EMG-based control for an upper-limb power-assist exoskeleton robot. *IEEE Trans SystMan Cybern B Cybern.* **2012**, *42*, 1064–1071. doi: 10.1109/TSMCB.2012.2185843

43. Kim, S.; Nussbaum, M. A.; Jia, B. The benefits of an additional worker are task-dependent: Assessing low-back injury risks during prefabricated (panelized) wall construction. *Appl Ergon.* **2012**, *43*(5), 843-849.
44. Kröger, T. Opening the door to new sensor-based robot applications—The Reflexxes Motion Libraries. *IEEE International Conference on Robotics and Automation, IEEE.* **2011** May, 1-4.
45. Le, P.; Best, T. M.; Khan, S.N.; Mendel, E.; Marras, W.S. A review of methods to assess coactivation in the spine. *J Electromyogr Kinesiol.* **2017** Feb, *32*, 51-60. doi: 10.1016/j.jelekin.2016.12.004. Epub 2016 Dec 20. PMID: 28039769.
46. Lee, K.S.; Lee, J.H. A study of efficiency of two-man lifting work. *Int J Ind Ergon.* **2001**, *28*(3– 4), 197–202.
47. Lee, T. H. Maximum isometric lifting strengths of men in teamwork. *Hum factors.* **2004**, *46*(4), 686-696.
48. Lenz, C.; Nair, S.; Rickert, M.; Knoll, A.; Rosel, W.; Gast, J.; Bannat, A.; Wallhoff, F. Joint-action for humans and industrial robots for assembly tasks. In *RO-MAN 2008-The 17th IEEE International Symposium on Robot and Human Interactive Communication.* IEEE. **2008**, August,130–135, 2008, doi:10.1109/ROMAN.2008.4600655.
49. Lewek, M. D.; Rudolph, K. S., Snyder-Mackler, L. Control of Frontal Plane Knee Laxity During Gait in Patients with Medial Compartment Knee Osteoarthritis. *Osteoarthr Cartil.* **2004**, *12* (9), 745–751.
50. Lobov, S.; Krilova, N.; Kastalskiy, I.; Kazantsev, V.; Makarov, V.A. Latent factors limiting the performance of sEMG-interfaces. *Sensors* **2018**, *18*, 1122. doi: 10.3390/s18041122
51. Lotti, N.; Xiloyannis, M.; Durandau, G.; Galofaro, E.; Sanguineti, V.; Masia, L.; Sartori, M. Adaptive Model-Based Myoelectric Control for a SoftWearable Arm Exosuit: A New Generation of Wearable Robot Control. *IEEE Robot. Autom. Mag.* **2020**, *27*, 43–53.
52. Macaluso, A.; Nimmo, M. A.; Foster, J. E.; Cockburn, M.; McMillan, N. C.; De Vito, G. Contractile Muscle Volume and Agonist–Antagonist Coactivation Account for Differences in Torque Between Young and Older Women. *Muscle Nerve.* **2002**, *25* (6), 858–863.
53. Marras, W.S.; Davis, K.G. A non-MVC EMG normalization technique for the trunk musculature: Part 1. Method development. *J Electromyogr Kinesiol.* **2001**, *11*, 1–9.
54. Marras, W.S.; Granata, K.P. Spine loading during trunk lateral bending motions. *J Biomech.* **1996**, *30*, 697–703. [https://doi.org/10.1016/S0021-9290\(97\)00010-9](https://doi.org/10.1016/S0021-9290(97)00010-9).
55. Marras, W.S.; Mirka, G.A. Electromyographic studies of the lumbar trunk musculature during the generation of low level trunk acceleration. *J Orthop Res.* 1993, *11* (6), 811–817. <https://doi.org/10.1002/jor.1100110606>
56. Ogenyi, U. E.; Liu, J.; Yang, C.; Ju, Z.; Liu, H. Physical Human-Robot Collaboration: Robotic Systems, Learning Methods, Collaborative Strategies, Sensors, and Actuators. *IEEE Trans Cybern.* **2021** Apr, *51*(4), 1888-1901. doi:10.1109/TCYB.2019.2947532. Epub 2021 Mar 17. PMID: 31751257.
57. Paolillo, A.; Colella, F.; Nosengo, N.; Schiano, F.; Stewart, W.; Zambrano, D.; Chappuis, I.; Lalive R.; Floreano, D. How to compete with robots by assessing job automation risks and resilient alternatives. *Sci Robot.* **2022**, *7*(65), eabg5561.
58. Papakostas, N.; Michalosa, G.; Makrisa, S.; Zouzias, D.; Chryssolouris, G. Industrial applications with cooperating robots for the flexible assembly. *Int. Journal of Computer Integrated Manufacturing.* **2011**, *24*(7), 650-660.
59. Paulíková, A.; Gyurák Babel'ová, Z.; Ubárová, M. Analysis of the Impact of Human-Cobot Collaborative Manufacturing Implementation on the Occupational Health and Safety and the Quality Requirements. *Int J Environ Res Public Health.* **2021** Feb 17, *18*(4):1927. doi: 10.3390/ijerph18041927. PMID: 33671204; PMCID: PMC7922989.
60. Ranavolo, A. Principi di Elettromiografia di Superficie. Dal Potenziale D'azione alle Applicazioni nei Diversi Settori Della Medicina e Dell'ingegneria. *Edizioni Universitarie Romane: Rome, Italy,* **2021**.
61. Ranavolo, A.; Ajoudani, A.; Cherubini, A.; Bianchi, M.; Fritzsche, L.; Iavicoli, S.; Sartori, M.; Silveti, A.; Vanderborght, B.; Varrecchia, T.; Draicchio, F. The Sensor-Based Biomechanical Risk Assessment at the Base of the Need for Revising of Standards for Human Ergonomics. *Sensors (Basel)* **2020a** Oct 10, *20*(20), 5750. doi: 10.3390/s20205750. PMID: 33050438; PMCID: PMC7599507.
62. Ranavolo, A.; Draicchio, F.; Varrecchia, T.; Silveti, A.; Iavicoli, S. Erratum: Alberto, R. et al., Wearable Monitoring Devices for Biomechanical Risk Assessment at Work: Current Status and Future Challenges-A Systematic Review. *Int. J. Environ. Res. Public Health* **2018b**, *15*, 2001. *Int J Environ Res Public Health.* 2018 Nov 16; *15*(11):2569. doi: 10.3390/ijerph15112569. Erratum for: *Int J Environ Res Public Health.* **2018** Sep 13, *15*(9), PMID: 30453581; PMCID: PMC6265804.
63. Ranavolo, A.; Mari, S.; Conte, C.; Serrao, M.; Silveti, A.; Iavicoli, S.; Draicchio, F. A new muscle co-activation index for biomechanical load evaluation in work activities. *Ergonomics* **2015**, *58* (6), 966-979.

64. Ranavolo, A.; Serrao, M.; Draicchio, F. Critical Issues and Imminent Challenges in the Use of sEMG in Return-To-Work Rehabilitation of Patients Affected by Neurological Disorders in the Epoch of Human-Robot Collaborative Technologies. *Front Neurol.* **2020b** Dec 22, *11*, 572069.
65. Ranavolo, A.; Varrecchia T, Rinaldi M, Silvetti A, Serrao M, Conforto S, Draicchio F. Mechanical lifting energy consumption in work activities designed by means of the "revised NIOSH lifting equation". *Ind Health* **2017**, *55* (5), 444-454.
66. Ranavolo, A.; Varrecchia, T.; Iavicoli, S.; Marchesi, A.; Rinaldi, M.; Serrao, M.; Conforto, S.; Cesarelli, M.; Draicchio, F. Surface electromyography for risk assessment in work activities designed using the “revised NIOSH lifting equation”. *Int. J. Ind. Ergon.* **2018a**, *68*, 34–45.
67. Roche, A.D.; Rehbaum, H.; Farina, D.; Aszmann, O.C. Prosthetic myoelectric control strategies: a clinical perspective. *Curr Surg Rep.* **2014**, *2*, 44. doi: 10.1007/s40137-013-0044-8
68. Rota, S.; Rogowski, I.; Champely, S.; Hautier, C. Reliability of EMG normalisation methods for upper-limb muscles. *J Sports Sci.* **2013**, *31*(15), 1696-704. doi: 10.1080/02640414.2013.796063. Epub 2013 May 22. PMID: 23697512.
69. Salvini, P.; Nicolescu, M.; Ishiguro, H. Benefits of human–robot interaction. *IEEE Robot Autom Mag.* **2011** Dec, *18*(4), 98–99.
70. Schwab, K. The fourth industrial revolution. *Currency.* **2017**.
71. Schwartz, C.; Tubez, F.; Wang, F.C.; Croisier, J.L.; Brüls, O.; Denoël, V.; Forthomme, B. Normalizing shoulder EMG: An optimal set of maximum isometric voluntary contraction tests considering reproducibility. *J Electromyogr Kinesiol.* **2017** Dec, *37*, 1-8. doi: 10.1016/j.jelekin.2017.08.005. Epub 2017 Aug 18. PMID: 28841523
72. Shi, J.; Jimmerson, G.; Pearson, T.; Menassa, R. Levels of human and robot collaboration for automotive manufacturing. *Workshop on Performance Metrics for Intelligent Systems, PerMIS.* **2012**, 95-100.
73. Sophia project. Available online: www.project-sophia.eu (accessed on 04 May 2022).
74. Tarbouriech, S.; Navarro, B.; Fraisse, P.; Crosnier, A.; Cherubini, A.; Sallé, D. "An admittance based hierarchical control framework for dual-arm cobots", *Mechatronics (to appear)*. *Mechatronics (to appear)*.
75. Van Der Beek, A.J.; Dennerlein, J.T.; A Huysmans, M.; Mathiassen, S.E.; Burdorf, A.; Van Mechelen, W.; van Dieën, J.H.; Frings-Dresen, M.H.; Holtermann, A.; Janwantanakul, P.; van der Molen, H. F.; Rempel, D.; Straker, L.; Walker-Bone, K.; Coenen, P. A research framework for the development and implementation of interventions preventing work-related musculoskeletal disorders. *Scand J Work Environ Heal.* **2017**, *43*(6), 526–539. doi: 10.5271/sjweh.3671.
76. van der Molen, H. F.; Visser, S.; Kuijper, P. P. F. M.; Faber, G.; Hoozemans, M. J.; van Dieën, J. H.; Frings-Dresen, M. H. The evaluation of team lifting on physical work demands and workload in ironworkers. *Work.* **2012**, *41*(Supplement 1), 3771-3773.
77. Varrecchia, T.; Conforto, S.; De Nunzio, A.M.; Draicchio, F.; Falla, D.; Ranavolo, A. Trunk Muscle Coactivation in People with and without Low Back Pain during Fatiguing Frequency-Dependent Lifting Activities. *Sensors (Basel).* **2022** Feb 12, *22*(4), 1417. doi: 10.3390/s22041417.
78. Varrecchia, T.; De Marchis, C.; Draicchio, F.; Schmid, M.; Conforto, S.; Ranavolo, A. Lifting activity assessment using kinematic features and neural networks. *Appl. Sci.* **2020**, *10*, 1989. Available online: <https://doi.org/10.3390/app10061989> (accessed on 15 September 2020).
79. Varrecchia, T.; De Marchis, C.; Rinaldi, M.; Draicchio, F.; Serrao, M.; Schmid, M.; Conforto, S.; Ranavolo, A. Lifting activity assessment using surface electromyographic features and neural networks. *Int. J. Ind. Ergon.* **2018**, *66*, 1–9.
80. Varrecchia, T.; Ranavolo, A.; Conforto, S.; De Nunzio, A.M.; Arvanitidis, M.; Draicchio, F.; Falla, D. Bipolar versus high-density surface electromyography for evaluating risk in fatiguing frequency-dependent lifting activities. *Appl Ergon.* **2021** Sep, *95*, 103456. doi: 10.1016/j.apergo.2021.103456.
81. Vera-Garcia, F.J.; Moreside, J.M.; McGill, S.M. MVC techniques to normalize trunk muscle EMG in healthy women. *J Electromyogr Kinesiol.* **2010**, *20*, 10–16.
82. Winter, D.A. Biomechanics and Motor Control of Human Movement, fourth ed. John Wiley & Sons, Inc, University of Waterloo, Waterloo, Ontario, Canada. **2009**.
83. World Robotics, Executive Summary -World Robotics 2019 Industrial Robots. **2019**, 13–16. Available Online: [https://ifr.org/downloads/press2018/Executive Summary WR 2019 Industrial Robots.pdf](https://ifr.org/downloads/press2018/Executive%20Summary%20WR%202019%20Industrial%20Robots.pdf).